Metabolomics (2018) 14:5
https://doi.org/10.1007/s11306-017-1304-x

ORIGINAL ARTICLE

Absolute quantitative lipidomics reveals lipidome-wide alterations in aging brain

Jia Tu[1,2] · Yandong Yin[1] · Meimei Xu[1,2] · Ruohong Wang[1,2] · Zheng-Jiang Zhu[1]

Received: 31 July 2017 / Accepted: 22 November 2017 / Published online: 28 November 2017

Abstract

Introduction The absolute quantitation of lipids at the lipidome-wide scale is a challenge but plays an important role in the comprehensive study of lipid metabolism.

Objectives We aim to develop a high-throughput quantitative lipidomics approach to enable the simultaneous identification and absolute quantification of hundreds of lipids in a single experiment. Then, we will systematically characterize lipidome-wide changes in the aging mouse brain and provide a link between aging and disordered lipid homeostasis.

Methods We created an in-house lipid spectral library, containing 76,361 lipids and 181,300 MS/MS spectra in total, to support accurate lipid identification. Then, we developed a response factor-based approach for the large-scale absolute quantifications of lipids.

Results Using the lipidomics approach, we absolutely quantified 1212 and 864 lipids in human cells and mouse brains, respectively. The quantification accuracy was validated using the traditional approach with a median relative error of 12.6%. We further characterized the lipidome-wide changes in aging mouse brains, and dramatic changes were observed in both glycerophospholipids and sphingolipids. Sphingolipids with longer acyl chains tend to accumulate in aging brains. Membrane-esterified fatty acids demonstrated diverse changes with aging, while most polyunsaturated fatty acids consistently decreased.

Conclusion We developed a high-throughput quantitative lipidomics approach and systematically characterized the lipidome-wide changes in aging mouse brains. The results proved a link between aging and disordered lipid homeostasis.

Keywords Lipidomics · Mass spectrometry · Absolute quantitation · Aging · Lipid homeostasis

1 Abbreviations

aLPC	Plasmanyl-lysoglycerophosphatidylcholine
Car	Carnitine
CE	Cholesteryl ester
Cer	Ceramide
CerP	Ceramide-1-phosphate
CL	Cardiolipin
DG	Diacylglycerol
GM1	G_{M1} ganglioside
Hex2Cer	Dihexosylceramide
HexCer	Hexosylceramide
LPA	Lysoglycerophosphatidic acid
LPC	Lysoglycerophosphatidylcholine
LPE	Lysoglycerophosphatidylethanolamine
LPG	Lysoglycerophosphatidylglycerol
LPI	Lysoglycerophosphatidylinositol
LPS	Lysoglycerophosphatidylserine
MG	Monoacylglycerol
PA	Glycerophosphatidic acid
PC	Glycerophosphatidylcholine
PE	Glycerophosphatidylethanolamine
PG	Glycerophosphatidylglycerol
PhytoCer	Phytoceramide
PhytoSph	Phytosphingosine
PI	Glycerophosphatidylinositol

Electronic supplementary material The online version of this article (https://doi.org/10.1007/s11306-017-1304-x) contains supplementary material, which is available to authorized users.

✉ Zheng-Jiang Zhu
jiangzhu@sioc.ac.cn

[1] Interdisciplinary Research Center on Biology and Chemistry, Shanghai Institute of Organic Chemistry, Chinese Academy of Sciences, Shanghai 200032, People's Republic of China

[2] University of Chinese Academy of Sciences, Beijing 100049, People's Republic of China

PIP2	Glycerophosphoinositol bisphosphate
pLPE	Plasmenyl-lysoglycerophosphatidylethanolamine
pPC	Plasmenyl-glycerophosphatidylcholine
pPE	Plasmenyl-glycerophosphatidylethanolamine
PS	Glycerophosphatidylserine
S1P	Sphingosine-1-phosphate
SM	Sphingomyelin
Sph	Sphinganine
ST	Sulfatide
TG	Triacylglycerol

2 Introduction

Lipids play numerous functions in physiology, such as energy storage, constitution of cell membranes, and cellular signaling, as well as in many diseases, such as cancer, neurodegenerative diseases, and cardiovascular disease (Wenk 2010; Han 2016; Rohrig and Schulze 2016). The comprehensive study of the roles and functions of lipids in molecular biology requires accurate identification and quantification of lipid species. The high structural diversity of lipids (e.g., > 40,000 lipids in the LIPID MAPS) presents a significant challenge for lipidomics (Fahy et al. 2009; van Meer 2005). The first popular mass spectrometry (MS)-based lipidomics technique, namely, shotgun lipidomics, was introduced by Han and Gross in 2003 (Han and Gross 2003). The method employs direct infusion to introduce lipids into a mass spectrometer (mostly triple quadrupole instrument) combined with either precursor ion scanning (PIS) or neutral loss scanning (NLS) (Han and Gross 2005). Later, a direct infusion approach with data-dependent acquisition using high-resolution MS was developed (Schwudke et al. 2006). Hundreds of lipids from complex biological samples can be directly identified and quantified without any chromatographic separation. However, this method is limited by ion suppression and the lack of discrimination between isomeric lipid species (Kofeler et al. 2012). Alternatively, coupling of liquid chromatographic (LC) separation to data-dependent MS/MS acquisition for lipidomics can effectively reduce matrix effects and resolve isobaric lipids (Cajka and Fiehn 2014; Sandra et al. 2010). The acquired MS/MS spectra provide rigorous identification of lipids through a spectral match with a standard or predicted MS/MS spectral library (Ivanisevic et al. 2013; Cajka and Fiehn 2017). Recently, a large-scale predicted MS/MS spectral library, LipidBlast, was developed to facilitate lipid identification using LC–MS/MS (Kind et al. 2013).

Absolute quantitation of a wide range of lipids is another challenge for lipidomics that is highly important for its applications in biological and clinical research (Lam et al. 2017; Heymsfield et al. 2015). Traditional approaches, such as multiple-reaction monitoring (MRM)-based targeted lipidomics, shotgun lipidomics or LC–MS/MS-based lipidomics, use lipids with odd-chain fatty acids or stable isotope-labeled internal standards (SIL-IS) to quantify a class of lipid (Shui et al. 2010; Ejsing et al. 2006; Heymsfield et al. 2015). However, only limited internal standards are available for many lipid classes. Recently, an alternative approach was developed to use a single SIL-IS and response factors (RFs) for simultaneous quantitation of multiple lipid classes; the quantitation accuracy is comparable to an MRM-based targeted approach (Cifkova et al. 2012). However, the method was only applied to limited lipid classes. Therefore, the absolute quantitation of lipids at the lipidome-wide scale is still very challenging and not yet readily realized.

In this work, we first developed a large-scale and absolute quantitative lipidomics approach, which enables the simultaneous identification and absolute quantitation of hundreds of lipids in a single experiment. The workflow is characterized by three features: (1) it embeds an in-house lipid MS/MS spectral library, containing 76,361 lipids and 181,300 MS/MS spectra, which provides accurate lipid identifications; (2) it supports the absolute quantitation of hundreds to thousands of lipids in one experiment using a single SIL-IS lipid; and (3) all identifications and quantifications are automatically achieved in one step. Using this lipidomics approach, we globally analyzed the lipidomes for various biological samples and absolutely quantified up to 1212 and 864 lipids in human cells and mouse brains, respectively. The quantitative accuracy was compared to the traditional approach with a median relative error (MRE) of 12.6%. The inter-day reproducibility was determined with a median relative standard deviation (RSD) of 14.4% over several weeks.

Aging is characterized by a physiological decline in various biological functions towards high risk for many diseases, such as neurodegenerative diseases, and eventually death (Lopez-Otin et al. 2013; Wyss-Coray 2016; Ivanisevic et al. 2016). Discovering the molecular basis of aging is one of the greatest challenges and interests in the field. Many studies have discovered that lipids are associated with aging and age-related neurodegenerative diseases, such as Alzheimer's disease (AD) (Lam et al. 2016; Xiang et al. 2015; Atherton et al. 2009; Shmookler Reis et al. 2011). Previous studies have demonstrated that the level of cholesterol and sphingolipids in the cerebral cortex progressively increased in an age-dependent manner (Cutler et al. 2004). Several findings also disclosed the abnormality of sphingolipid metabolism in the brain of AD patients (Touboul and Gaudin 2014; Han 2010). Additionally, a set of glycerophospholipids were reported as potential biomarkers of the diagnosis of preclinical AD (Mapstone et al. 2014). In this work, we further applied our absolute quantitative lipidomics to reveal the lipidome-wide consequences of aging in mouse brains. Dramatic changes were observed in lipid profiles, such as the

age-dependent reduction in glycerophospholipids and the increase in sphingolipids. Interestingly, the changes in sphingolipids occurred in an acyl-chain length-dependent manner with aging. The absolute quantitative analysis of membrane-esterified fatty acids further validated their dependency with aging. For example, the major components of polyunsaturated fatty acids (PUFAs, C20:3, C20:4, C22:5 and C22:6) in glycerophospholipids were preferentially reduced in old mouse brains. Thus, with our developed large-scale and absolute quantitative lipidomics approach, we systematically characterized lipidome-wide alterations in mouse brain during aging and identified a link between aging and disordered lipid homeostasis.

3 Materials and methods

Lipids from human plasma, Jurkat cells and mouse brains were extracted using a modified MTBE extraction method (Matyash et al. 2008). Detailed descriptions of chemicals, sample preparation, LC–MS/MS data acquisition, curation of an in-house MS/MS spectral library, and calculation of recovery rate are provided in the Supplementary Information.

3.1 Measurements of response factor values

The response factor is defined as a relationship between the SIL-IS and an individual lipid class. To obtain the RF values, we first measured the linear standard curves of 34 lipid standards with our chosen SIL-IS [d7-PE (15:0/18:1)]. Second, we calculated the RF value according to Eq. 1, referring to the ratio between the slope of the SIL-IS-based calibration curve and the slope of the lipid standard-based calibration curves. Experiments were independently analyzed at least two to three times over several months to obtain reproducible RF values (Supplementary Table 1). RF values were expected to range from 0.1 to 10. However, several lipid classes [carnitine (Car), monoacylglycerol (MG), sphingosine-1-phosphate (SIP), GM1 ganglioside (GM1) and cholesteryl ester (CE)], with RF values outside this range, were removed from the quantitation. Finally, a total of 29 lipid classes were simultaneously absolutely quantified with only one SIL-IS using the RF-based approach. For each lipid class, the appropriate polarity and ion adducts were selected for sensitive quantitation (Supplementary Table 1).

$$RF_{lipid} = Slope_{IS}/Slope_{lipid} \quad (1)$$

3.2 Data processing

An in-house program, namely, LipidAnalyzer, was developed using R for automatic data analysis. The raw data files (.wiff format) were converted to files in mzXML format using the "msconvert" program from ProteoWizard (version 3.0.6150). Then, the mzxML files were loaded into LipidAnalyzer for data processing. Peak detection was first applied to the MS1 data. The CentWave algorithm in XCMS was used for peak detection (Tautenhahn et al. 2008). The parameter "peakwidth" was set as (5, 25) in units of seconds, referring to the minimum and maximum peak widths for peak detection. The parameter ''snthresh'' is set as 3 for sensitive peak detection. For multiple LC–MS data files, an ordered bijective interpolated warping (OBI-Warp) algorithm in XCMS was used for peak alignment (Prince and Marcotte 2006). The CAMERA package is used for peak annotation (Kuhl et al. 2012). As a result, a peak table including *m/z*, retention time (RT), and peak area information was generated.

Next, we extracted the MS/MS spectra for each feature according to the *m/z* and RT. If one precursor ion is fragmented multiple times, the MS/MS spectrum closest to the peak apex was extracted and subjected to de-noising processing. Specifically, fragment ions in the MS/MS spectrum with an intensity of less than 30 counts or less than 3% of the most abundant fragment ions (except precursor ion) were discarded. In addition, satellite ions (due to the ringing effect) close to the main peak with a mass difference of less than 0.3 Da and a relative intensity of less than 20% were also removed. With the MS/MS spectrum, lipid identification was achieved through a spectral match using an in-house MS/MS spectral library. First, an accurate mass match was performed to search all lipid species in the library with a mass tolerance of 25 ppm. Next, for each matched lipid, the corresponding experimental MS/MS spectrum was used to calculate the similarity to the MS2 spectrum in the library. A similarity score was calculated using the dot product function (Eq. 2) (Stein and Scott 1994).

$$\text{Similarity Score} = \frac{\sum \left(\left([\mathrm{I}]_L^n \, [\mathrm{mz}]_L^m \right) \left([\mathrm{I}]_E^n \, [\mathrm{mz}]_E^m \right) \right)}{\sqrt{\sum \left([\mathrm{I}]_L^n [\mathrm{mz}]_L^m \right)^2 \sum \left([\mathrm{I}]_E^n \, [\mathrm{mz}]_E^m \right)^2}} \quad (2)$$

where mz and I refer to the mass-to-charge value and intensity from the library (L) or experimental (E) data, respectively, while m and n represent the weight of mz and intensity, respectively. Here, we set m = 1 and n = 0.6 (positive mode) or 1 (negative mode). The similarity score ranges from 0 to 1, referring to no similarity and a perfect match, respectively. Lipid matches with scores larger than 0.8 were kept as true identifications. The values for the weights of mz (m) and intensity (n) are optimized systematically, as shown in Supplementary Fig. S1.

Finally, the absolute quantitation of lipids can be achieved using the peak area, SIL-IS and RF information (Eq. 3).

$$C_{lipid} = C_{IS} \times \frac{A_{lipid}}{A_{IS}} \times RF_{lipid} \quad (3)$$

3.3 Animals

Forty mice (c57BL/6J strain, SPF level) at five different ages (4, 12, 24, 32 to 52 weeks, n = 8 in each group) were purchased from the HFK Bioscience Company (Beijing, China). Mice were anesthetized with isoflurane and sacrificed by cervical dislocation. Heads were removed using a surgical scissor. The skulls were freed by flipping the skin and cut through the most anterior part. The parietal bones were tilted and broken off. The brains were freed from meninges and removed from the skull. Brains were washed to wipe off excess blood and immediately collected for storage at − 80 °C.

4 Results and discussion

To enable a fully automated approach towards the identification and absolute quantification of lipids, we developed an integrated workflow to process multi-dimensional LC–MS/MS data files (Fig. 1), including the following steps: (1) Perform peak detection and alignment on MS1 data to form an MS1 peak table with m/z, RT and peak area information. (2) For each peak, automatically extract the corresponding MS/MS spectrum and match with our in-house MS/MS spectral library for lipid identification. A similarity score of a spectral match above 0.8 was regarded as true identification. (3) Lipid absolute quantification is further achieved using peak area, its corresponding RF for the identified lipid class and SIL-IS information. This unattended workflow is highly-efficient, requiring ~ 1 h to simultaneously identify and absolutely quantify hundreds of lipids from ten LC–MS/MS data files.

4.1 Curation of an in-house MS/MS library for accurate lipid identification

Fragmentation in MS/MS spectra is significantly influenced by the instrument platform and level of collision energy (Supplementary Fig. S2). We also found that publicly available lipid MS/MS spectral libraries such as LipidBlast are not suitable for inter-lab applications (Supplementary Fig. S3). Therefore, curation of an in-house library is necessary to improve the accuracy of lipid identification. An experimental workflow to curate an in-house MS/MS spectral library is illustrated in Fig. 2a and Supplementary Fig. S4, including three major steps: (1) acquisition of standard MS/MS spectra, (2) generation of rules for fragmentation and relative intensities, and (3) prediction of the MS/MS spectral library with the generated rules. More detailed descriptions are provided in the Supplementary Information. In total, our in-house MS/MS spectral library includes 34 lipid classes, 76,361 lipids, and 181,300 predicted MS/MS spectra

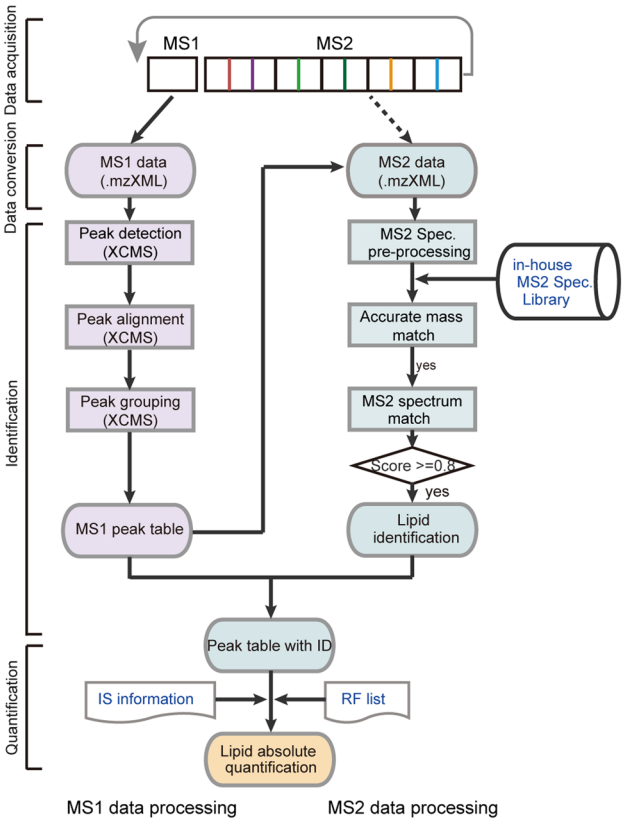

Fig. 1 Schematic illustration of the workflow for automated lipid identification and absolute quantification from multiple LC–MS/MS data files

(Fig. 2b and Supplementary Table 2). Compared to LipidBlast, our in-house library has a broader coverage of lipid classes (Supplementary Table 3). MS/MS spectra for several common adductive forms, including $[M+H]^+$, $[M+NH4]^+$, $[M+Na]^+$, $[M-H]^-$, and $[M+HCOO]^-$, were also provided in our library.

To demonstrate the advantages of our in-house MS/MS library in lipid identification, we compared the performance of our library with that of LipidBlast. Commercially available glycerophospholipid mixtures were used to estimate the number of true positive and false positive identifications of lipids. As shown in Fig. 2c, the use of our in-house MS/MS library provides more true positive identifications in both positive and negative modes compared to LipidBlast, while both libraries have similar numbers of false positive identifications (Supplementary Fig. S5). In addition, various biological samples, including human plasma, Jurkat cells and mouse brain samples, were used to estimate the coverage of both libraries for lipid identification. As shown in Fig. 2d, the use of our in-house library provides 1000–1800 lipid identifications for positive and negative modes, which is generally 60–100% more than found using LipidBlast (600–1100 lipids in total). In addition, we also found that

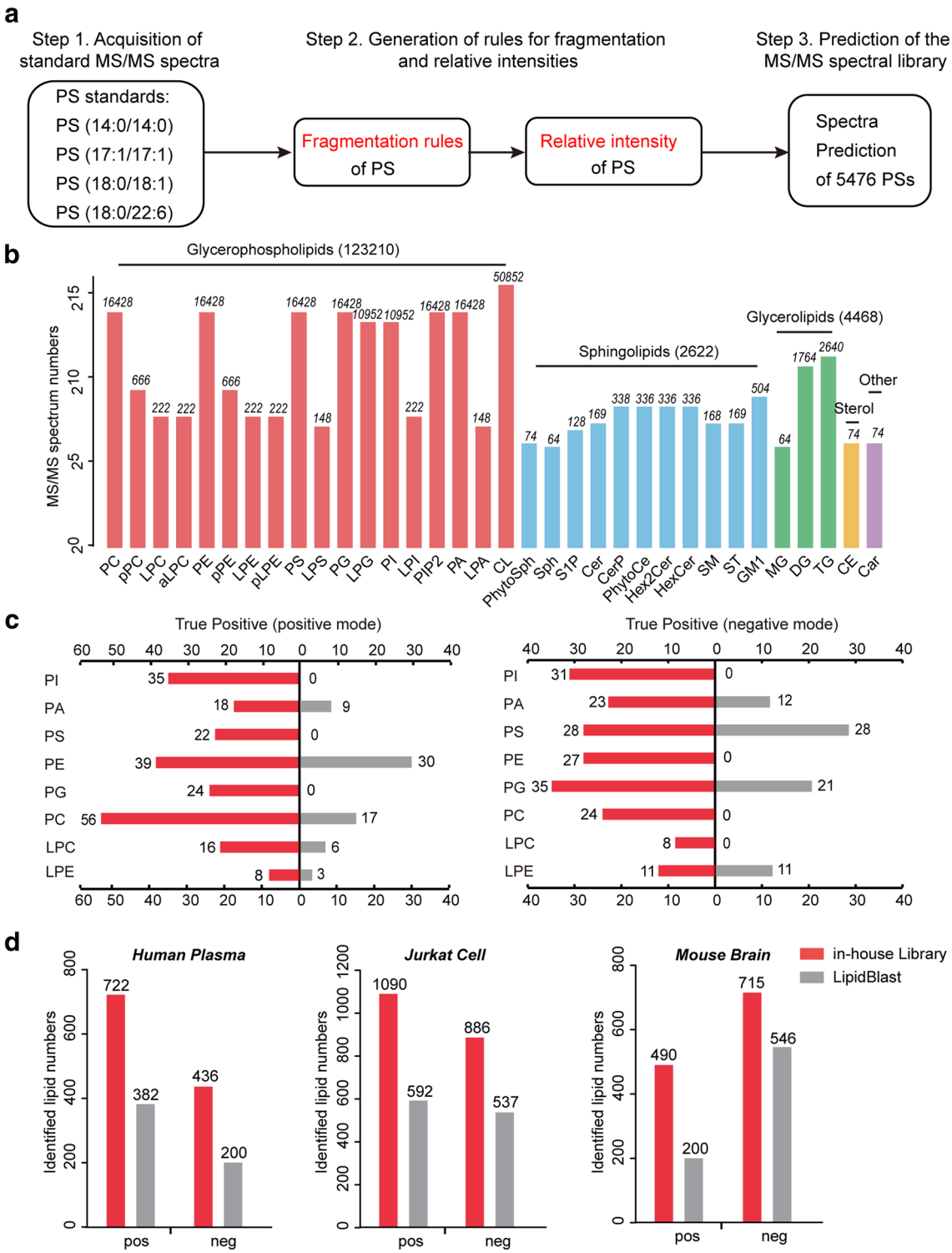

Fig. 2 Curation of an in-house MS/MS spectral library for accurate lipid identification. **a** The experimental workflow to predict the MS/MS spectra for PS lipids. **b** Numbers for MS/MS spectra in our in-house MS/MS library. **c** Comparison of the true positive identifications of lipids using either in-house MS/MS library or LipidBlast in both positive and negative modes. **d** Comparison of the identified lipid numbers of various biological samples (n = 10) using either our in-house MS/MS library or LipidBlast

our in-house library provides accurate lipid identification and is able to distinguish structural and positional lipid isomers. For example, using the different relative intensities derived from the sn1/sn2 position, it readily identified the unknown lipid as PS (18:0/20:3) (score: 0.995) and not the positional isomer PS (20:3/18:0) (score: 0.885) (Supplementary Fig. S6a). For comparison, LipidBlast cannot differentiate the sn1/sn2 positional isomers (Supplementary Fig. S6b). In summary, our in-house library provides high coverage, accurate lipid identifications for various complex biological samples.

4.2 Development of the RF-based approach for absolute quantitation

Several experimental factors are critically important for the development of the RF-based approach towards absolute quantitation of lipids (Lam et al. 2017), including the choice of SIL-IS, the reproducibility of RF values, and the recovery rate. First, we chose a single standard lipid [d7-PE (15:0/18:1)] as SIL-IS (Fig. 3a). There is no ion interference in various biological samples and it provides good ionization responses in both positive and negative modes. Then, we experimentally measured the linear calibration curves of 34 lipid classes using this SIL-IS. Most lipids have quantitative dynamic ranges ranging from 1 to 5000 ng/ml, while some lipids have narrower ranges (Supplementary Fig. S7). Using calibration curves, RF values for 34 lipid classes were calculated and are provided in Supplementary Table 1. Most RF values range from 0.1 to 10 and qualified for absolute quantitation (Fig. 3b). However, several lipid classes, such as Car, MG, SIP, GM1 and CE, have RF values out of the expected range and are removed from quantitative analysis. We also demonstrated that RF values have good reproducibility over several months, with a median RSD of 14% (Supplementary Fig. S8). Therefore, a total of 29 lipid classes can be simultaneously absolutely quantified with only one SIL-IS lipid, combined with the RF-based approach, which

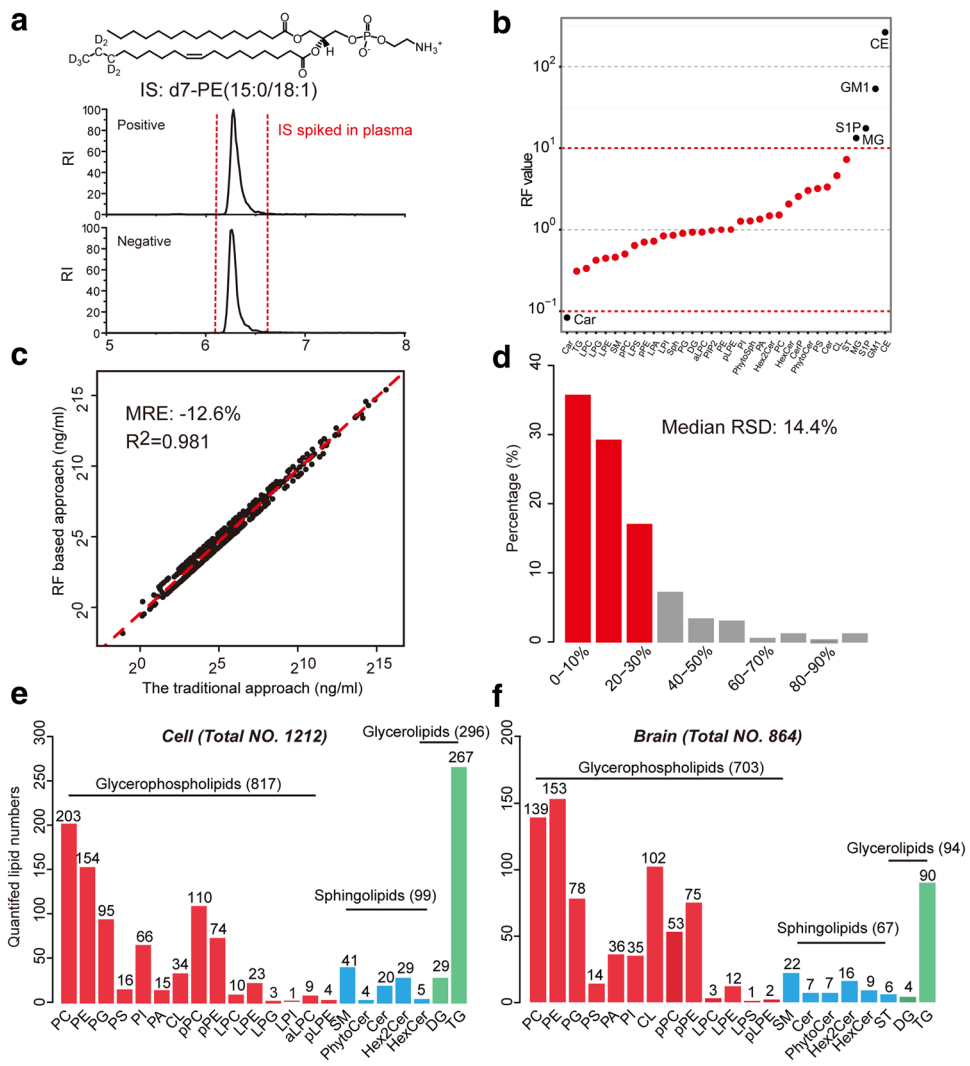

Fig. 3 **a** Chosen internal standard d7-PE (15:0/18:1) for absolute quantitation. **b** Values of RF for 34 lipid classes. **c** Correlation between concentrations of 406 plasma lipids obtained from the RF-based approach and traditional approach. **d** Inter-day reproducibility for lipid species in human plasma measured at three different time points (n = 3). **e**–**f** Bar plots for numbers of quantified lipids in Jurkat cell or mouse brain samples (n = 10 in each group)

enables large-scale absolute quantification. To ensure the accurate absolute quantitation of various classes of lipids, we evaluated the recovery rate of each lipid class by spiking 34 lipids in a ^{13}C-labled bacteria sample. The results showed that recovery rates of lipids are mostly in the interval of 60–140%, except S1P, phytosphingosine (PhytoSph) and lysoglycerophosphatidylinositol (LPI), which have relatively low recovery rates (Supplementary Fig. S9).

We further evaluated the accuracy and inter-day reproducibility of RF-based quantification. We compared the absolute concentrations of 406 lipid species (covering 7 lipid classes) in human plasma using the RF-based approach and the traditional approach. The traditional approach requires the addition of the corresponding SIL-IS (Supplementary Table 4) for each lipid class (Fig. 3c). The regression coefficient is 0.98, and the MRE is 12%, which demonstrated that the RF-based approach has a comparable quantitation accuracy to the traditional approach. Additionally, the inter-day reproducibility for individual lipid species was determined with a median RSD of 14.4% over several weeks, and 82.3% of lipid species were within RSD < 30% (Fig. 3d).To assess the coverage of lipid quantitation, we globally analyzed various biological samples, and absolutely quantified up to 1212 and 864 lipids in Jurkat cell and mouse brain samples, respectively, covering 23 different lipid classes (Fig. 3e–f). The coverage of quantified lipid species is much higher than in previous publications (Sales et al. 2017; Zhang et al. 2015; Yang et al. 2009).

4.3 Global lipidomics analysis of mouse brain during aging

Using the above workflow, we performed global lipidomic profiling on mouse brain tissues at five different ages (4, 12, 24, 32, and 52 weeks). In total, 1430 lipid species (605 lipids in positive mode, 825 in negative mode) were identified. Among them, 992 lipid species were absolutely quantified, covering 22 lipid classes (Supplementary Fig. S10).

With the absolute quantities of lipids, we first calculated the mass percentages of the quantified 22 lipid classes in mouse brain (Fig. 4a and Supplementary Fig. S11). Obviously, the mass percentages of total glycerophospholipids consistently decreased in the brain with age, while the mass percentages of total sphingolipids showed an increasing trend with age. Age-related changes in individual lipid classes were further analyzed and plotted in Fig. 4b. Similarly, most glycerophospholipids such as cardiolipin (CL), glycerophosphatidylglycerol (PG), glycerophosphatidic acid (PA), glycerophosphatidylserine (PS), glycerophosphatidylethanolamine (PE), glycerophosphatidylcholine (PC) and glycerophosphatidylinositol (PI) were clustered together, demonstrating a gradually decreasing trend with age. For example, the amount of PIs significantly decreased by 86.9% from week 4 to week 52. An appreciable accumulation of sphingolipids, such as ceramide (Cer), phytoceramide (PhytoCer), hexosylceramide (HexCer) and sulfatide (ST), was observed at week 52. For example, the amount of HexCers increased by 169% from week 4 to week 52. One possible reason is impaired sphingolipid-to-glycerophospholipid metabolism during aging. Another proposed interpretation may be derived from the competitive usage of acyl-CoAs (Kihara 2014) during aging. Acyl-CoAs are common substrates for energy production, which can be either esterified to form membrane glycerophospholipids or incorporated into Cers to form sphingolipids (Cooper et al. 2015). Acyl-CoAs may be incorporated to produce more sphingolipids in old mouse brains.

To analyze the trends for individual lipid species with age, we categorized lipids based on their similarities in temporal variation. In a Kruskal–Wallis test analysis, 311 of 992 lipids have p values less than 0.001 among the five ages and were further selected for hierarchical clustering analysis (Fig. 4c). Six distinct lipid clusters were clearly defined and demonstrated diverse temporal changes with aging (Fig. 4d and Supplementary Fig. S12). Among them, lipids in clusters B and D were found to consistently increase or decrease with age, respectively. The lipids within each cluster demonstrated a diverse composition, suggesting that clustered lipids might be co-regulated or functionally related. Interestingly, sphingolipids showed an acyl-chain-length-dependent change with age. Specifically, sphingolipids such as sphingomyelin (SM), HerCer, Cer and PhytoCer in cluster B preferentially contain a longer acyl-chain ranging from C20 to C26. Conversely, sphingolipids in cluster D mostly contain the shorter acyl-chain. For example, HexCer(d18:1/24:1) and SM(d16:1/26:1) were significantly higher at week 52, up to 227 and 84% increases compared to the levels at week 4, respectively. In contrast, HexCer(d18:1/18:0) and SM(d18:1/18:1) were significantly lower at week 52 and dropped by 14 and 41% compared to the levels at week 4 (Fig. 4e).

4.4 Alterations in fatty acid composition with age

We further studied the absolute quantities of 791 membrane-esterified fatty acids in glycerophospholipids across five ages (Fig. 5a and Supplementary Fig. S13). The highly abundant fatty acids, such as C18:1, C18:0, C16:0, C20:4, and C22:6, account for approximately 70% of all fatty acids in glycerophospholipids. Among the saturated fatty acids (SFAs), the levels of C16:0 and C18:0 have no significant differences with age (Supplementary Fig. S14). The levels of C20:0 and C22:0 were significantly higher in week 52 than in week 12, up to 65 and 18% increases, respectively. For monounsaturated fatty acids (MUFAs), the levels of C20:1 and C22:1 were significantly increased in week 52 relative

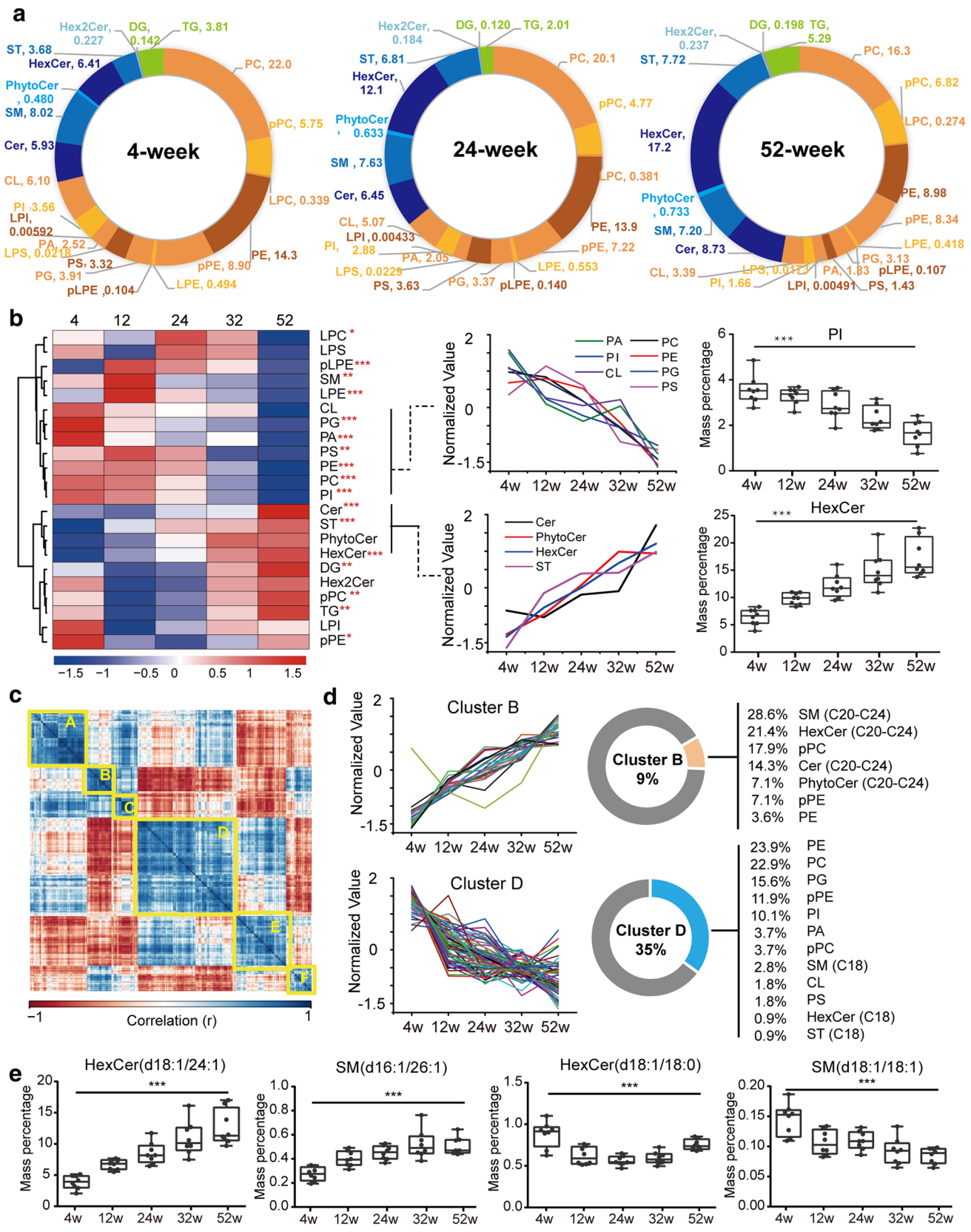
a
4-week
Hex2Cer, 0.227
DG, 0.142
TG, 3.81
ST, 3.68
HexCer, 6.41
PC, 22.0
PhytoCer, 0.480
SM, 8.02
pPC, 5.75
Cer, 5.93
CL, 6.10
LPC, 0.339
PI, 3.56
LPI, 0.00592
PA, 2.52
LPS, 0.0218
PS, 3.32
PE, 14.3
PG, 3.91
pPE, 8.90
pLPE, 0.104
LPE, 0.494
24-week
Hex2Cer, 0.184
DG, 0.120
TG, 2.01
ST, 6.81
PC, 20.1
HexCer, 12.1
pPC, 4.77
PhytoCer, 0.633
SM, 7.63
LPC, 0.381
Cer, 6.45
PE, 13.9
CL, 5.07
LPI, 0.00433
PI, 2.88
pPE, 7.22
PA, 2.05
LPS, 0.0229
LPE, 0.553
PS, 3.63
PG, 3.37
pLPE, 0.140
52-week
Hex2Cer, 0.237
DG, 0.198
TG, 5.29
ST, 7.72
PC, 16.3
pPC, 6.82
HexCer, 17.2
LPC, 0.274
PE, 8.98
PhytoCer, 0.733
pPE, 8.34
SM, 7.20
LPE, 0.418
Cer, 8.73
PG, 3.13
CL, 3.39
LPS, 0.0173
PA, 1.83
pLPE, 0.107
PI, 1.66
LPI, 0.00491
PS, 1.43
b
4 12 24 32 52
LPC*
LPS
pLPE***
SM**
LPE***
CL
PG***
PA***
PS**
PE***
PC***
PI***
Cer***
ST***
PhytoCer
HexCer***
DG**
Hex2Cer
pPC**
TG**
LPI
pPE*
−1.5 −1 −0.5 0 0.5 1 1.5
Normalized Value
PA PC PI PE CL PG PS
4w 12w 24w 32w 52w
Mass percentage
PI
***
Cer PhytoCer HexCer ST
HexCer
c
A
B
C
D
E
F
−1
Correlation (r)
1
d
Cluster B
Normalized Value
4w 12w 24w 32w 52w
Cluster B 9%
28.6% SM (C20-C24)
21.4% HexCer (C20-C24)
17.9% pPC
14.3% Cer (C20-C24)
7.1% PhytoCer (C20-C24)
7.1% pPE
3.6% PE
Cluster D
Cluster D 35%
23.9% PE
22.9% PC
15.6% PG
11.9% pPE
10.1% PI
3.7% PA
3.7% pPC
2.8% SM (C18)
1.8% CL
1.8% PS
0.9% HexCer (C18)
0.9% ST (C18)
e
HexCer(d18:1/24:1)
SM(d16:1/26:1)
HexCer(d18:1/18:0)
SM(d18:1/18:1)
Mass percentage
***
4w 12w 24w 32w 52w

◂**Fig. 4** **a** Pie diagrams for mass percentages of 22 quantified lipid classes (992 lipids) in mouse brain across different ages. **b** Clusters of different lipid classes according to hierarchical clustering. The changing trends of clustered lipid classes with age were also provided. **c** Correlation matrix of dysregulated lipid species (p value < 0.001, 311 lipids in total) during aging. **d** Age-dependent trend for lipid species in clusters B and D. **e** Sphingolipids with different acyl-chain lengths show an opposite trend with age

to those in week 12 mice, up by 62 and 101%, respectively. In contrast, the level of C18:1 decreased by 13% in week 52 mice. Interestingly, a consistent decrease in PUFAs, such as C20:3 (14%), C20:4 (25%), C22:5 (31%) and C22:6 (2%), was observed at week 52 compared to week 4 (Fig. 5b). The level of C22:6 was first elevated in week 12 and continually decreased with age. In summary, old mouse brains demonstrated both increased membrane-esterified fatty acids, including SFAs (C20:0 and C22:0) and MUFAs (C20:1 and C22:1), and significantly decreased levels of PUFAs (C20:3, C20:4, C22:5, and C22:6). PUFAs are susceptible to lipid peroxidation (Xu et al. 2009; Sultana et al. 2013), and the decrease in PUFAs may greatly alter the physicochemical properties of cell membranes during aging, resulting in severe cellular dysfunction. A significant reduction in the levels of PUFAs such as C20:3 and C20:4 has been reported in the brain tissues of AD patients (Snowden et al. 2017). These results proved that temporal changes in fatty acid composition in the aging brain are caused by dysregulated lipid metabolism and may significantly contribute to the pathogenesis of age-dependent neurodegenerative diseases.

5 Conclusions

In conclusion, we developed a large-scale lipidomics workflow for the simultaneous identification and absolute quantification of hundreds to thousands of lipids in biological samples. Our approach has comparable accuracy in quantitation to the traditional approach. With the availability of automatic data analysis software, the identification and absolute quantification of lipids was readily achieved in a high-efficient and automatic manner. We applied this workflow to reveal lipidome-wide consequences of aging in mouse brains. Dramatic changes were observed in brain lipid profiles during aging, with significant reductions in glycerophospholipids and increased sphingolipids. Interestingly, sphingolipids exhibited an acyl-chain-length-dependent change with age. Specifically, sphingolipids with longer acyl-chains tend to accumulate in brains with aging, while those with shorter acyl-chains tend to decrease with aging. The levels of membrane-esterified fatty acids perform diverse temporal changes, while most polyunsaturated fatty acids consistently decrease with aging. These results illustrate a link between aging and dysregulated lipid metabolism in the aging mouse

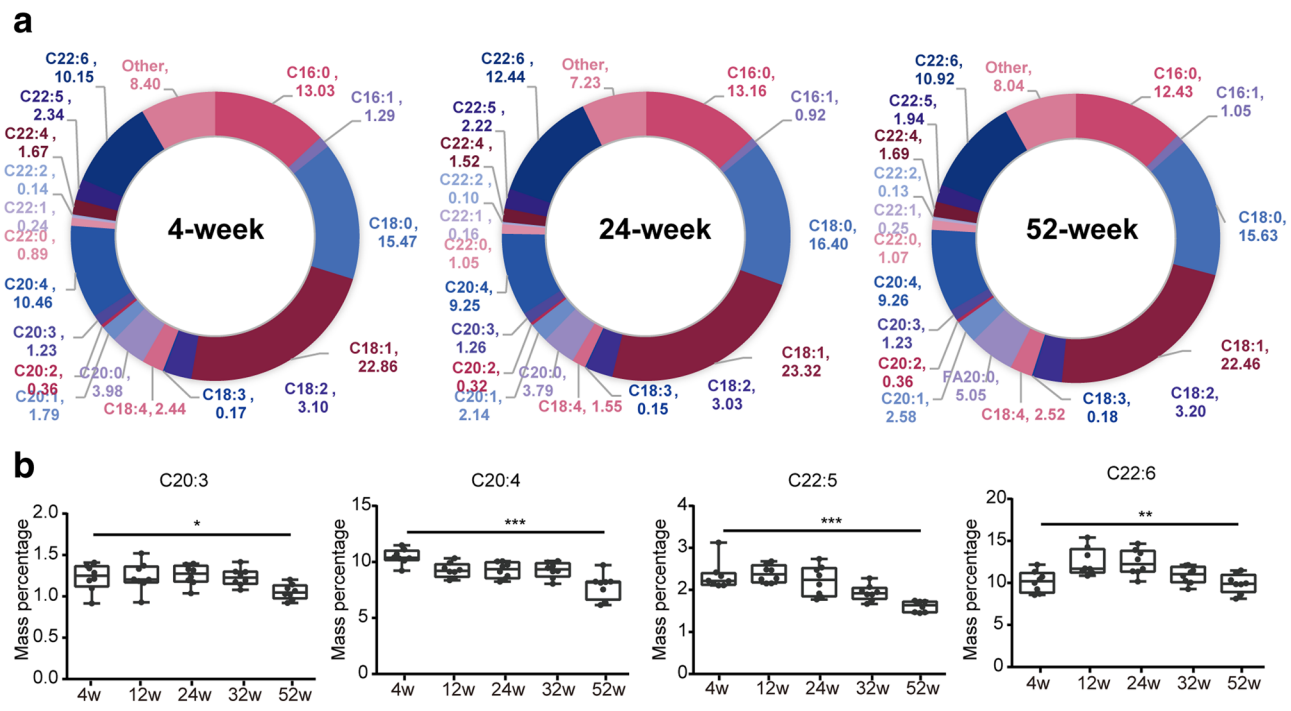

Fig. 5 **a** Pie diagrams for mass percentages of 791 membrane-esterified fatty acids in glycerophospholipids across different ages. **b** Age-dependent decrease in specific membrane-esterified PUFAs with aging

brain and will significantly contribute to understanding the pathogenesis of age-dependent neurodegenerative diseases.

In this work, we demonstrated high-throughput identification and absolute quantification of lipids on a lipidome-scale level. However, it should be noted that the lipid identification in the work is only maintained at the level 2 according to the Metabolomics Standards Initiative (MSI) (Salek et al. 2013; Sumner et al. 2007). As considering the confidence level of identification is critical for lipidomics, we suggest one should use the purchased/synthesized lipid standard to achieve the highest level of identification especially when one lipid is considered to be extremely important (e.g. as a biomarker for disease diagnosis). Alternatively, other orthogonal information, such as retention time (RT) on the chromatographic separation (Aicheler et al. 2015; Broeckling et al. 2016) or collision cross section (CCS) from ion mobility-mass spectrometry (Zhou et al. 2017) can be readily predicted to provide better confidence in lipid identification. Therefore, a combination of accurate mass, MS/MS spectrum, CCS and RT will be very significant to improve the identification accuracy in the near future.

Acknowledgements The work is financially supported by National Natural Science Foundation of China (Grant No. 21575151). Z.-J. Z. is supported by Thousand Youth Talents Program from Government of China.

Compliance with ethical standards

Conflict of interest All authors declare no competing financial interest.

Ethical approval All institutional and national guidelines for the care and use of biological samples were followed. The data were acquired in accordance with appropriate ethical requirements. No human study was involved in this work. All experiments on mice were conducted according to the protocols approved by Animal Care Committee of the Interdisciplinary Research Center on Biology and Chemistry (IRCBC), Chinese Academy of Sciences (CAS).

References

Aicheler, F., Li, J., Hoene, M., Lehmann, R., Xu, G., & Kohlbacher, O. (2015). Retention time prediction improves identification in nontargeted lipidomics approaches. *Analytical Chemistry, 87*(15), 7698–7704. https://doi.org/10.1021/acs.analchem.5b01139.

Atherton, H. J., Gulston, M. K., Bailey, N. J., Cheng, K. K., Zhang, W., Clarke, K., et al. (2009). Metabolomics of the interaction between PPAR-alpha and age in the PPAR-alpha-null mouse. *Molecular Systems Biology, 5*, 259. https://doi.org/10.1038/msb.2009.18.

Broeckling, C. D., Ganna, A., Layer, M., Brown, K., Sutton, B., Ingelsson, E., et al. (2016). Enabling efficient and confident annotation of LC-MS metabolomics data through MS1 spectrum and time prediction. *Analytical Chemistry, 88*(18), 9226–9234. https://doi.org/10.1021/acs.analchem.6b02479.

Cajka, T., & Fiehn, O. (2014). Comprehensive analysis of lipids in biological systems by liquid chromatography-mass spectrometry. *Trends in Analytical Chemistry, 61*, 192–206. https://doi.org/10.1016/j.trac.2014.04.017.

Cajka, T., & Fiehn, O. (2017). LC-MS-based lipidomics and automated identification of lipids using the lipidblast in-silico MS/MS library. *Methods in Molecular Biology, 1609*, 149–170. https://doi.org/10.1007/978-1-4939-6996-8_14.

Cifkova, E., Holcapek, M., Lisa, M., Ovcacikova, M., Lycka, A., Lynen, F., et al. (2012). Nontargeted quantitation of lipid classes using hydrophilic interaction liquid chromatography-electrospray ionization mass spectrometry with single internal standard and response factor approach. *Analytical Chemistry, 84*(22), 10064–10070. https://doi.org/10.1021/ac3024476.

Cooper, D. E., Young, P. A., Klett, E. L., & Coleman, R. A. (2015). physiological consequences of compartmentalized acyl-CoA metabolism. *Journal of Biological Chemistry, 290*(33), 20023–20031. https://doi.org/10.1074/jbc.R115.663260.

Cutler, R. G., Kelly, J., Storie, K., Pedersen, W. A., Tammara, A., Hatanpaa, K., et al. (2004). Involvement of oxidative stress-induced abnormalities in ceramide and cholesterol metabolism in brain aging and Alzheimer's disease. *Proceedings of the National Academy of Sciences USA, 101*(7), 2070–2075. https://doi.org/10.1073/pnas.0305799101.

Ejsing, C. S., Duchoslav, E., Sampaio, J., Simons, K., Bonner, R., Thiele, C., et al. (2006). Automated identification and quantification of glycerophospholipid molecular species by multiple precursor ion scanning. *Analytical Chemistry, 78*(17), 6202–6214. https://doi.org/10.1021/ac060545x.

Fahy, E., Subramaniam, S., Murphy, R. C., Nishijima, M., Raetz, C. R., Shimizu, T., et al. (2009). Update of the LIPID MAPS comprehensive classification system for lipids. *Journal of Lipid Research, 50*(Suppl), 9–14, https://doi.org/10.1194/jlr.R800095-JLR200.

Han, X. (2010). The pathogenic implication of abnormal interaction between apolipoprotein E isoforms, amyloid-beta peptides, and sulfatides in Alzheimer's disease. *Molecular Neurobiology, 41*(2–3), 97–106. https://doi.org/10.1007/s12035-009-8092-x.

Han, X. (2016). Lipidomics for studying metabolism. *Nature Reviews Endocrinology, 12*(11), 668–679. https://doi.org/10.1038/nrendo.2016.98.

Han, X., & Gross, R. W. (2003). Global analyses of cellular lipidomes directly from crude extracts of biological samples by ESI mass spectrometry: A bridge to lipidomics. *Journal of Lipid Research, 44*(6), 1071–1079. https://doi.org/10.1194/jlr.R300004-JLR200.

Han, X., & Gross, R. W. (2005). Shotgun lipidomics: Electrospray ionization mass spectrometric analysis and quantitation of cellular lipidomes directly from crude extracts of biological samples. *Mass Spectrometry Reviews, 24*(3), 367–412. https://doi.org/10.1002/mas.20023.

Heymsfield, S. B., Hu, H. H., Shen, W., & Carmichael, O. (2015). Emerging technologies and their applications in lipid compartment measurement. *Trends in Endocrinology & Metabolism, 26*(12), 688–698. https://doi.org/10.1016/j.tem.2015.10.003.

Ivanisevic, J., Stauch, K. L., Petrascheck, M., Benton, H. P., Epstein, A. A., Fang, M., et al. (2016). Metabolic drift in the aging brain. *Aging (Albany NY), 8*(5), 1000–1020. https://doi.org/10.18632/aging.100961.

Ivanisevic, J., Zhu, Z. J., Plate, L., Tautenhahn, R., Chen, S., O'Brien, P. J., et al. (2013). Toward 'omic scale metabolite profiling: A dual separation-mass spectrometry approach for coverage of lipid and central carbon metabolism. *Analytical Chemistry, 85*(14), 6876–6884. https://doi.org/10.1021/ac401140h.

Kihara, A. (2014). Sphingosine 1-phosphate is a key metabolite linking sphingolipids to glycerophospholipids. *Biochimica et Biophysica Acta, 1841*(5), 766–772. https://doi.org/10.1016/j.bbalip.2013.08.014.

Kind, T., Liu, K. H., Lee, D. Y., DeFelice, B., Meissen, J. K., & Fiehn, O. (2013). LipidBlast in silico tandem mass spectrometry database

for lipid identification. *Nature Methods, 10*(8), 755–758. https://doi.org/10.1038/nmeth.2551.

Kofeler, H. C., Fauland, A., Rechberger, G. N., & Trotzmuller, M. (2012). Mass spectrometry based lipidomics: An overview of technological platforms. *Metabolites, 2*(1), 19–38. https://doi.org/10.3390/metabo2010019.

Kuhl, C., Tautenhahn, R., Bottcher, C., Larson, T. R., & Neumann, S. (2012). CAMERA: An integrated strategy for compound spectra extraction and annotation of liquid chromatography/mass spectrometry data sets. *Analytical Chemistry, 84*(1), 283–289. https://doi.org/10.1021/ac202450g.

Lam, S. M., Chua, G. H., Li, X. J., Su, B., & Shui, G. (2016). Biological relevance of fatty acyl heterogeneity to the neural membrane dynamics of rhesus macaques during normative aging. *Oncotarget, 7*(35), 55970–55989. https://doi.org/10.18632/oncotarget.11190.

Lam, S. M., Tian, H., & Shui, G. (2017). Lipidomics, en route to accurate quantitation. *Biochimica et Biophysica Acta, 1862*(8), 752–761. https://doi.org/10.1016/j.bbalip.2017.02.008.

Lopez-Otin, C., Blasco, M. A., Partridge, L., Serrano, M., & Kroemer, G. (2013). The hallmarks of aging. *Cell, 153*(6), 1194–1217. https://doi.org/10.1016/j.cell.2013.05.039.

Mapstone, M., Cheema, A. K., Fiandaca, M. S., Zhong, X., Mhyre, T. R., MacArthur, L. H., et al. (2014). Plasma phospholipids identify antecedent memory impairment in older adults. *Nature Medicine, 20*(4), 415–418. https://doi.org/10.1038/nm.3466.

Matyash, V., Liebisch, G., Kurzchalia, T. V., Shevchenko, A., & Schwudke, D. (2008). Lipid extraction by methyl-tert-butyl ether for high-throughput lipidomics. *Journal of Lipid Research, 49*(5), 1137–1146. https://doi.org/10.1194/jlr.D700041-JLR200.

Prince, J. T., & Marcotte, E. M. (2006). Chromatographic alignment of ESI-LC-MS proteomics data sets by ordered bijective interpolated warping. *Analytical Chemistry, 78*(17), 6140–6152. https://doi.org/10.1021/ac0605344.

Rohrig, F., & Schulze, A. (2016). The multifaceted roles of fatty acid synthesis in cancer. *Nature Reviews Cancer, 16*(11), 732–749. https://doi.org/10.1038/nrc.2016.89.

Salek, R. M., Steinbeck, C., Viant, M. R., Goodacre, R., & Dunn, W. B. (2013). The role of reporting standards for metabolite annotation and identification in metabolomic studies. *Gigascience, 2*(1), 13. https://doi.org/10.1186/2047-217X-2-13.

Sales, S., Knittelfelder, O., & Shevchenko, A. (2017). Lipidomics of human blood plasma by high-resolution shotgun mass spectrometry. *Methods in Molecular Biology, 1619*, 203–212. https://doi.org/10.1007/978-1-4939-7057-5_16.

Sandra, K., Ados, P., Vanhoenacker, S., David, G., F., & Sandra, P. (2010). Comprehensive blood plasma lipidomics by liquid chromatography/quadrupole time-of-flight mass spectrometry. *Journal of Chromatography A, 1217*(25), 4087–4099. https://doi.org/10.1016/j.chroma.2010.02.039.

Schwudke, D., Oegema, J., Burton, L., Entchev, E., Hannich, J. T., Ejsing, C. S., et al. (2006). Lipid profiling by multiple precursor and neutral loss scanning driven by the data-dependent acquisition. *Analytical Chemistry, 78*(2), 585–595. https://doi.org/10.1021/ac051605m.

Shmookler Reis, R. J., Xu, L., Lee, H., Chae, M., Thaden, J. J., Bharill, P., et al. (2011). Modulation of lipid biosynthesis contributes to stress resistance and longevity of *C. elegans* mutants. *Aging (Albany NY), 3*(2), 125–147. https://doi.org/10.18632/aging.100275.

Shui, G., Guan, X. L., Gopalakrishnan, P., Xue, Y., Goh, J. S., Yang, H., et al. (2010). Characterization of substrate preference for Slc1p and Cst26p in Saccharomyces cerevisiae using lipidomic approaches and an LPAAT activity assay. *PLoS ONE, 5*(8), e11956. https://doi.org/10.1371/journal.pone.0011956.

Snowden, S. G., Ebshiana, A. A., Hye, A., An, Y., Pletnikova, O., O'Brien, R., et al. (2017). Association between fatty acid metabolism in the brain and Alzheimer disease neuropathology and cognitive performance: A nontargeted metabolomic study. *PLoS Medicine, 14*(3), e1002266. https://doi.org/10.1371/journal.pmed.1002266.

Stein, S. E., & Scott, D. R. (1994). Optimization and testing of mass spectral library search algorithms for compound identification. *Journal of the American Society for Mass Spectrometry, 5*(9), 859–866. https://doi.org/10.1016/1044-0305(94)87009-8.

Sultana, R., Perluigi, M., & Allan Butterfield, D. (2013). Lipid peroxidation triggers neurodegeneration: A redox proteomics view into the Alzheimer disease brain. *Free Radical Biology and Medicine, 62*, 157–169. https://doi.org/10.1016/j.freeradbiomed.2012.09.027.

Sumner, L. W., Amberg, A., Barrett, D., Beale, M. H., Beger, R., Daykin, C. A., et al. (2007). Proposed minimum reporting standards for chemical analysis Chemical Analysis Working Group (CAWG) Metabolomics Standards Initiative (MSI). *Metabolomics, 3*(3), 211–221. https://doi.org/10.1007/s11306-007-0082-2.

Tautenhahn, R., Bottcher, C., & Neumann, S. (2008). Highly sensitive feature detection for high resolution LC/MS. *BMC Bioinformatics, 9*, 504. https://doi.org/10.1186/1471-2105-9-504.

Touboul, D., & Gaudin, M. (2014). Lipidomics of Alzheimer's disease. *Bioanalysis, 6*(4), 541–561. https://doi.org/10.4155/bio.13.346.

van Meer, G. (2005). Cellular lipidomics. *The EMBO Journal, 24*(18), 3159–3165. https://doi.org/10.1038/sj.emboj.7600798.

Wenk, M. R. (2010). Lipidomics: New tools and applications. *Cell, 143*(6), 888–895. https://doi.org/10.1016/j.cell.2010.11.033.

Wyss-Coray, T. (2016). Ageing, neurodegeneration and brain rejuvenation. *Nature, 539*(7628), 180–186. https://doi.org/10.1038/nature20411.

Xiang, Y., Lam, S. M., & Shui, G. (2015). What can lipidomics tell us about the pathogenesis of Alzheimer disease? *Biological Chemistry, 396*(12), 1281–1291. https://doi.org/10.1515/hsz-2015-0207.

Xu, L., Davis, T. A., & Porter, N. A. (2009). Rate constants for peroxidation of polyunsaturated fatty acids and sterols in solution and in liposomes. *Journal of the American Chemical Society, 131*(36), 13037–13044. https://doi.org/10.1021/ja9029076.

Yang, K., Cheng, H., Gross, R. W., & Han, X. (2009). Automated lipid identification and quantification by multidimensional mass spectrometry-based shotgun lipidomics. *Analytical Chemistry, 81*(11), 4356–4368. https://doi.org/10.1021/ac900241u.

Zhang, T., Chen, S., Liang, X., & Zhang, H. (2015). Development of a mass-spectrometry-based lipidomics platform for the profiling of phospholipids and sphingolipids in brain tissues. *Analytical and Bioanalytical Chemistry, 407*(21), 6543–6555. https://doi.org/10.1007/s00216-015-8822-z.

Zhou, Z., Tu, J., Xiong, X., Shen, X., & Zhu, Z. J. (2017). LipidCCS: Prediction of collision cross-section values for lipids with high precision to support ion mobility-mass spectrometry-based lipidomics. *Analytical Chemistry, 89*(17), 9559–9566. https://doi.org/10.1021/acs.analchem.7b02625.